Low-Velocity Impact Response of Laminated Plates

R. L. Ramkumar* and P. C. Chen†
Northrop Corporation, Hawthorne, California

An analysis is presented to predict the response of anisotropic laminated plates to low-velocity impact by a rigid object. Transverse shear deformation in the plates is accounted for using Mindlin's theory and the governing equations are solved using Fourier integral transforms, assuming infinite planform dimensions for the plate. The contact area is assumed to vary with time, and the complex contact problem is replaced by a loading history that is based on available experimental data from instrumented impact tests. Computed plate response is used to predict initial failures, including back surface fiber/matrix failures, directly below the impact site and internal delaminations. Analytical predictions are shown to compare well with available experimental results and finite element solutions.

Nomenclature

A_{ij}	= laminate in-plane stiffness matrix
a	= half the base length of the square contact area at $t=c$
B_{ij}	= laminate stiffness matrix that couples in-plane and flexural response
C_1	= contact force per unit time
$Ci(z)$	= cosine integral of z
c	= time corresponding to initial failure
D_{ij}	= laminate flexural stiffness matrix
h	= laminate thickness
K	= Mindlin shear correction factor
M_{ij}	= bending moment resultants
N_{ij}	= in-plane stress resultants
P	= mass per unit area
Q_{ij}	= elastic stiffness matrix for a layer
Q_x, Q_y	= transverse shear stress resultants
$Si(z)$	= sine integral of z
t	= time
w	= displacements in the z (thickness) direction
$w(\xi,\eta,t)$	= solution in the Fourier domain corresponding to $w(x,y,t)$
ψ_x, ψ_y	= bending slopes in the x-z, y-z planes
ρ	= mass per unit volume

Introduction

THE response of a laminated plate to low-velocity impact by a rigid object has been studied by many investigators.[1-9] The experimental investigation in Ref. 2 quantifies the effects of low-velocity impact damage on the static strength and lifetime of laminates that are representative of typical fighter aircraft wing skin layups. The results indicate that internal damage, with no visual indication on the outer surfaces, severely affects the compressive strength and lifetime of laminates. Low-velocity impact situations under which such damages are induced concern designers and maintenance personnel because routine visual inspection of laminated structural components may fail to detect these damages. Likewise, fiber failures and/or splitting between fibers on the back surface, away from the undamaged impacted surface, could also affect the strength and lifetime of the laminate. Computation of temporal and spatial stresses in the laminate and their incorporation into reliable failure criteria are essential for the prediction of the extent of low-velocity impact damage induced by a rigid body.

In most of the analyses attempted thus far,[3-9] the complex contact phenomenon is accounted for indirectly, the laminate is assumed to be orthotropic, the boundary conditions are assumed to be simple supports, and the temporal impact loads are assumed to act over a constant area. The analysis presented in this paper accounts for the anisotropy in the laminate, including bending-twisting coupling, and assumes the contact area to vary with time. The contact phenomenon is replaced by an equivalent loading history, and the planform plate dimensions are assumed to be infinite to simplify the analysis.

Analysis

The governing equations of motion for a laminated plate, subjected to an impact load on the top surface ($z=h/2$) and accounting for transverse shear deformation using Mindlin's theory, are[5]

$$KA_{55}(\psi_{x,x}+w,_{xx})+KA_{44}(\psi_{y,y}+w,_{yy}) = Pw,_{tt}-\sigma_z(x,y,h/2,t) \tag{1}$$

$$D_{11}\psi_{x,xx}+2D_{16}\psi_{x,xy}+D_{66}\psi_{x,yy}+D_{16}\psi_{y,xx} + (D_{12}+D_{66})\psi_{y,xy}+D_{26}\psi_{y,yy}-KA_{55}(\psi_x+w,_x)=0 \tag{2}$$

$$D_{16}\psi_{x,xx}+(D_{12}+D_{66})\psi_{x,xy}+D_{26}\psi_{x,yy}+D_{66}\psi_{y,xx} + 2D_{26}\psi_{y,xy}+D_{22}\psi_{y,yy}-KA_{44}(\psi_y+w,_y)=0 \tag{3}$$

In the above equations, in-plane displacements are assumed to be negligible in comparison to the transverse displacement w and rotatory inertia terms are not included. A_{ij} and D_{ij} are laminate in-plane and bending stiffnesses,[10] ψ_x and ψ_y are the midplane bending slopes in the x-z and y-z planes, K is the Mindlin shear correction factor ($=\pi^2/12$), and a comma after a symbol denotes differentiation with respect to the variables that follow the comma.

In Eq. (1), $\sigma_z(x, y, h/2, t)$ is the spatial and temporal impact stress distribution on the impacted surface ($z=h/2$). Based on the force-time traces obtained through instrumented impact tests[11] (see Fig. 1), it is assumed that impact force increases linearly with time up to initial failure (force $=C_1 t$). Initial failure is assumed to occur at time $t=c$. In the instrumented test record[11] (see Fig. 1), this is manifested as the first major unloading phenomenon in the impact force-time trace. The nature of the initial failure, however, can be ascertained only by computing the transient spatial stresses and incorporating

Presented as Paper 82-0750 at the AIAA/ASME/ASCE/AHS 23rd Structures, Structural Dynamics and Materials Conference, New Orleans, La., May 10-12, 1982; submitted May 12, 1982; revision submitted Dec. 7, 1982. Copyright © American Institute of Aeronautics and Astronautics, Inc., 1982. All rights reserved.

*Engineering Specialist, Structural Mechanics Research Department, Aircraft Division.

†Engineer, Dynamics Department, Aircraft Division.

them into appropriate failure criteria. The loading rate is dependent on the geometry of the laminate and the impactor, their material properties, the impact location, and the boundary constraints. For impactors with spherical tips, the contact radius is zero (point contact) when contact is just established. And, depending on various impact parameters (especially the impactor tip radius), the contact dimension increases as the impactor causes local inelastic deformation. This phenomenon eludes analytical prediction and involves an indeterminate contact problem, coupled with nonlinear anisotropic material behavior. The elliptical contact area is, therefore, approximated by a square whose base length increases linearly with time to a value of $2a$ at $t=c$. The linear variation of contact length with time is an unsubstantiated approximation assumed for mathematical convenience. In the published literature, a doubly elliptical spatial distribution of the normal stress over the contact region is commonly assumed. However, its validity remains to be established. In this paper the contact stress is simplified to be uniform over the time-varying contact area. With these assumptions, the spatial and temporal variation of contact stress is expressed as

$$\sigma_z(x,y,h/2,t) = -\left(\frac{C_I t}{4(at/c)^2}\right)XYT \tag{4}$$

where C_I is the rate of loading

$$\begin{aligned}
X(x,t) &= 1 \quad \text{for} \quad |x| < at/c \\
&= 0 \quad \text{for} \quad |x| \geq at/c \\
Y(y,t) &= 1 \quad \text{for} \quad |y| < at/c \\
&= 0 \quad \text{for} \quad |y| \geq at/c \\
T(t) &= 1 \quad \text{for} \quad t \leq c \\
&= 0 \quad \text{for} \quad t > c
\end{aligned} \tag{5}$$

and $2a$ is the base length of the contact area when initial failure occurs ($t=c$).

It must be noted here that the contact stress expressions in Eqs. (4) and (5) approximate the measured loading history[11] only until initial failure occurs at $t=c$. The total impulse due to the actual impact phenomenon is significantly underestimated. However, an accurate computation of the transient response of the impacted laminate up to $t=c$ will suffice to predict the nature and extent of the damage precipitated at $t=c$. Moreover, beyond $t=c$, the presence of the damage has to be appropriately incorporated into a modified analysis to

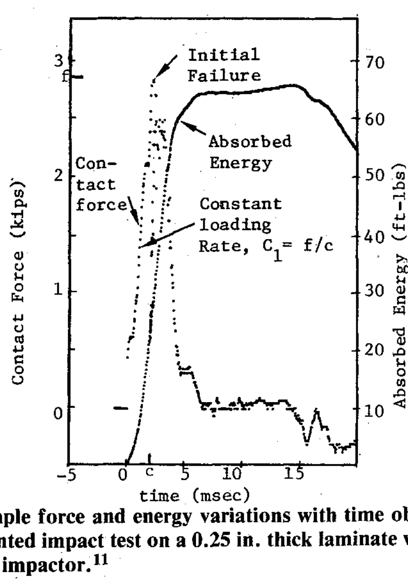

Fig. 1 Sample force and energy variations with time obtained from an instrumented impact test on a 0.25 in. thick laminate with a 0.5 in. tip diameter impactor.[11]

predict the response of the damaged laminate beyond initial failure. The laminate ceases to be a continuum and the analysis increases in complexity. Consequently, the analysis developed in this paper is valid only up to $t=c$ and is aimed at predicting the nature and extent of the initial damage.

Using Fourier integrals,[12] the governing equations are transformed from the x-y domain to the ξ-η Fourier domain. The transformed variables in the Fourier domain are $\bar{\tilde{w}}$, $\bar{\tilde{\psi}}_x$, and $\bar{\tilde{\psi}}_y$. A simultaneous solution of transformed Eqs. (2) and (3) yields the following relationships:

$$\bar{\tilde{\psi}}_x = \left(\frac{H_2H_9 - H_3H_6}{H_5H_9 - H_6^2}\right)\bar{\tilde{w}} \tag{6}$$

$$\bar{\tilde{\psi}}_y = \left(\frac{H_3H_5 - H_2H_6}{H_5H_9 - H_6^2}\right)\bar{\tilde{w}} \tag{7}$$

where the H_i are quadratic complex functions of ξ, η, and laminate properties, which are defined as

$$\begin{aligned}
H_1 &= -\xi^2 KA_{55} - \eta^2 KA_{44} \\
H_2 &= i\xi KA_{55} = -H_4 \\
H_3 &= i\eta KA_{44} = -H_7 \\
H_5 &= -\xi^2 D_{11} - 2\xi\eta D_{16} - \eta^2 D_{66} - KA_{55} \\
H_6 &= -\xi^2 D_{16} - \xi\eta(D_{12} + D_{66}) - \eta^2 D_{26} = H_8 \\
H_9 &= -\xi^2 D_{66} - 2\xi\eta D_{26} - \eta^2 D_{22} - KA_{44}
\end{aligned} \tag{8}$$

Substitution of Eqs. (6) and (7) into the transformed Eq. (1) results in the following second-order, ordinary differential equation in $\bar{\tilde{w}}$:

$$\bar{\tilde{w}}_{,tt} + \omega_n^2 \bar{\tilde{w}} = \frac{-C_I c^2}{Pa^2 \xi\eta t}\left[u(t) - u_c(t)\right] \frac{\sin\xi at}{c} \frac{\sin\eta at}{c} \tag{9}$$

where

$$\omega_n = \sqrt{-\frac{1}{P}\left(H_1 + \frac{H_3^2 H_9 + H_2^2 H_5 - 2H_2H_3H_6}{H_5H_9 - H_6^2}\right)} \tag{10}$$

Using the convolution integral, the solution to Eq. (9) is

$$\begin{aligned}
\bar{\tilde{W}}_{t\leq c} = \frac{-C_I c^2}{4Pa^2 \xi\eta\omega_n} \Big\{ & \sin(\omega_n t)\Big[Ci(|w_1 t|) + Ci(|w_2 t|) \\
& - Ci(|w_3 t|) - Ci(|w_4 t|) + \ln\left(\frac{|w_3||w_4|}{|w_1||w_2|}\right)\Big] \\
& + \cos(\omega_n t)\left[Si(w_4 t) - Si(w_3 t) - Si(w_2 t) + Si(w_1 t)\right]\Big\}
\end{aligned} \tag{11}$$

$$\begin{aligned}
\bar{\tilde{W}}_{t>c} = -\frac{C_I c^2}{p4a^2 \xi\eta\omega_n} \Big\{ & \sin(\omega_n t)\Big[Ci(|W_1 c|) + Ci(|W_2 c|) \\
& - Ci(|W_3 c|) - Ci(|W_4 c|) - \ln\left|\frac{W_1 W_2}{W_3 W_4}\right|\Big] \\
& + \cos(\omega_n t)\{Si(W_4 c) - Si(W_3 c) - Si(W_2 c) + Si(W_1 c)\}\Big\}
\end{aligned} \tag{12}$$

where $Si(z)$ and $Ci(z)$ are sine and cosine integrals of z, respectively, and

$$\begin{aligned}
w_1 &= \xi a/c - \eta a/c - \omega_n, \qquad & w_2 &= \xi a/c - \eta a/c + \omega_n \\
w_3 &= \xi a/c + \eta a/c - \omega_n, \qquad & w_4 &= \xi a/c + \eta a/c + \omega_n
\end{aligned} \tag{13}$$

Equations (6), (7), (11), and (12) provide the solutions for the bending slopes and the transverse displacement of the laminated plate in the Fourier (ξ-η) domain. Derivatives of these quantities are obtained through simple manipulations of the above expressions to yield the strains in the Fourier domain.[12] The transverse displacement w, the transverse shear stress resultant (Q_x or Q_y), and the strains in the bottom ply directly below the impact site are then transformed back to the x-y plane using a numerical inversion routine (FFTCC).[13]

Correlation Studies

The validity of the present analysis is established by comparing its predictions with experimental measurements and finite element solutions for a few test cases investigated by Ramkumar.[11] Tables 1 and 2 list the considered test cases and the relevant data. In Ref. 11, $[(\pm 45/0_2)_2/\pm 45/0/90]_{2S}$ AS/3501-6 graphite/epoxy laminates were subjected to low-velocity impact by spherical-tipped steel impactors in a drop tower. Test panels were 66 cm (26 in.) long and 25 cm (10 in.) wide and were bolted to steel substructures with 2.54 cm (1 in.) wide flanges prior to being impacted. Tests were instrumented to obtain the contact force variation during impact, and the gathered data were numerically integrated to compute the energy absorbed during impact (see Fig. 1). Assuming the steel indentor to be rigid, the contact force data were used to numerically compute the impactor displacement during the contact period. After impact, the panels were inspected visually and via ultrasonic through-transmission tests. Ultrasonic C-scan records provide a planform size of the internal damage in the impacted laminate, and B and three-dimensional scans illustrate the damage distribution in a three-dimensional manner (see Fig. 2). The planform dimensions and the depth of indentation at the impact site, corresponding to a midbay impact at the incipient damage energy level, were also recorded for the various tests. Subtracting the depth of indentation at $t=c$ from the computed impactor displacement at $x=y=0$ and $t=c$ (when initial failure occurred), the maximum displacement of the laminate at $t=c$ was obtained.

Table 1 Assumed laminate properties

Property	Laminate B[a]	Laminate A[a]
h, mm	12.700	6.350
D_{11}, kN-m	13.137	1.642
D_{12}, kN-m	3.382	0.423
D_{16}, kN-m	0.168	0.021
D_{22}, kN-m	5.799	0.725
D_{26}, kN-m	0.168	0.021
D_{66}, kN-m	3.645	0.456
A_{55}, MN/m	69.939	34.969
A_{44}, MN/m	69.939	34.969
K	0.8225	0.8225
P, kg/m^2	20.193	10.096
h_{ply},[b] mm	0.264	0.132

[a]Laminates A and B are 48-ply laminates with the following layup: $[(\pm 45/0_2)_2/\pm 45/0/90]_{2S}$. [b]$h_{ply}$ is the individual ply thickness of AS/3501-6 graphite/epoxy prepreg, 0.1321 mm for type I and 0.2642 mm for type II material.

Table 2 Test cases considered for correlation studies (from Ref. 11)[a]

Test case	h, mm	D, mm	C_I MN/s	c, ms	a, mm
1	6.35	3.18	4.092	1.25	0.25
2	6.35	12.7	5.738	2.20	6.35
3	6.35	50.8	6.050	2.40	17.78
4	12.7	12.7	23.353	1.25	6.35
5	12.7	50.8	26.511	1.45	17.78

[a]$h=6.35$ and 12.7 mm refer to laminates A and B, respectively, in Table 1. h is the total thickness of the laminate, D the tip diameter of the steel impactor, C_I the experimentally obtained loading rate, c the contact time corresponding to initial failure, and a half the base length of the approximate square contact area at $t=c$.

A finite element analysis was also carried out for a limited number of impact tests to permit a three-way correlation study. One quadrant of the impacted laminate was modeled, the transient loads to be imposed were obtained from the instrumented impact test data,[11] and the contact area was varied in accordance with the assumptions of the present analysis. NASTRAN was employed to obtain the finite element solutions.

Table 3 presents a three-way comparison among the analytical predictions, experimental measurements, and numerical (finite element) solutions. The maximum transverse displacement of the impacted laminates at $x=y=0$ (impact location), corresponding to the time when initial failure

Table 3 Predicted and measured plate displacements

	Maximum transverse plate displacement $w(0,0,-h/2,c)$, mm[a]		
Test case (see Table 2)	Analytical prediction	Experimental measurement[11]	Finite element solution
1	1.32	1.22	—
2	5.72	5.49	—
3	7.06	6.17	—
4	2.08	3.05	3.15
5	3.07	3.45	4.06

[a]$w(0,0,-h/2,c)$ corresponds to $x=y=0$ (impact location), $z=-h/2$ (bottom surface), and $t=c$.

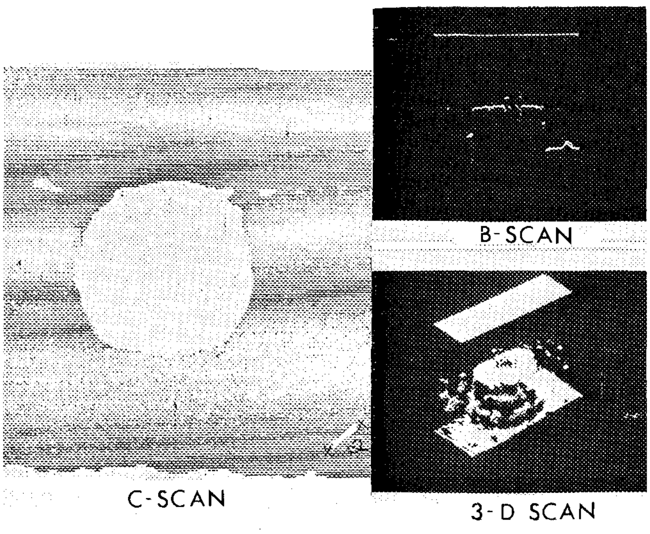

Fig. 2 Ultrasonic C, B, and three-dimensional scans of a typical impact-damaged laminate location.[11]

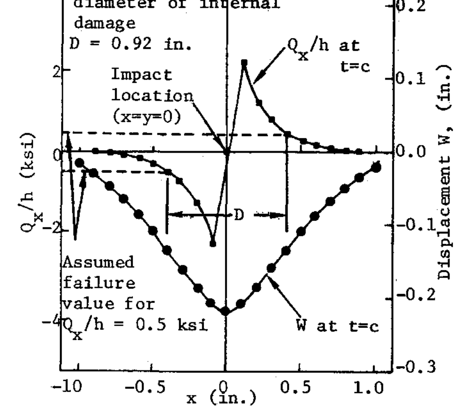

Fig. 3 Prediction of internal damage size for test case 2.

Table 4 Predicted and measured strains

	Longitudinal strain,[a] μmm/mm		Transverse strain,[a] μmm/mm	
Test case (see Table 2)	Analytical prediction	Experimental measurement[b]	Analytical prediction	Experimental measurement[b]
1	2850	2318	4,650	5,689
2	7252	6182	11,851	12,000
3	6725	5455	10,331	16,000
4	4052	4364	7,329	8,364

[a]Corresponds to $x=y=0$ (impact location), $z=-h/2$, and $t=c$. [b]Obtained from oscillograph records in Ref. 11.

Table 5 Predicted and observed failures

	Internal damage size (diameter in mm)		Flexural damage on the back surface[c]	
Test case (see Table 2)	Analytical prediction[a]	Experimental measurement[b]	Analytical prediction	Experimental observation
1	9.14	9.40	None	None
2	23.37	41.15	M	F.M
3	27.94	93.47	F,M	F,M
4	20.32	19.56	None	None

[a]Based on an assumed failure value of 3.45 MPa (0.5 ksi) for the transverse shear stress, Q_x/h.
[b]This is the approximate diameter of the damage as seen on the ultrasonic C-scan record.[11]
[c]M denotes matrix splitting between fibers on the back surface and F fiber failure on the back surface. F and M are precipitated when the strains along and perpendiculr to the fiber direction, in the bottom ply, exceed 12,200 and 5500 μmm/mm, respectively.

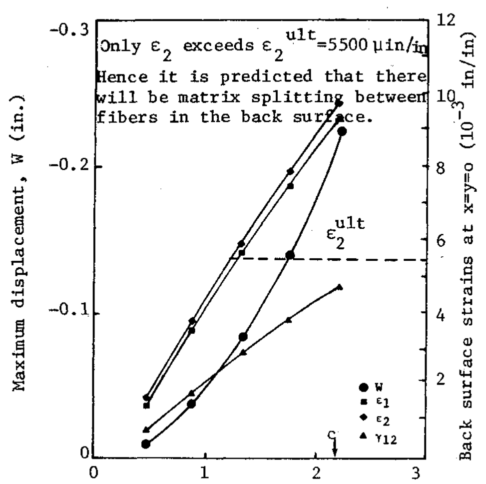

Fig. 4 Prediction of back surface failures for test case 2.

occurs ($t=c$), is chosen to be the basis for comparison. It is seen that the analytical predictions compare well with the experimental data in every case. For test cases 4 and 5, the finite element solutions are also in fair agreement with the analytical predictions and experimental measurements.

Table 4 presents a comparison between the analytically predicted and experimentally measured back surface ($z=-h/2$) strains at $t=c$ in the longitudinal and transverse directions of the impacted laminate. The strains correspond to locations in the back surface that are directly below the impact site. Again, the analytically predicted strains are seen to be in fair agreement with the experimental measurements for the considered test cases.

The capability of the analysis in predicting the type and extent of damage in the impacted laminate, at $t=c$, is addressed next. Assuming internal damage to be predominantly delaminations, the extent of internal damage was predicted based on an assumed failure value for Q_x/h—the transverse shear stress in the laminate.[8] Delaminations were assumed to extend from the impact site to the location where Q_x/h attained a value of 3.45 MPa (0.5 ksi), as shown in Fig. 3. The choice of the mentioned failure value was arbitrary and was selected to make the analytical predictions for the first test case agree well with the C-scan measurements in Ref. 11. On the back surface, computed strains were transformed to the fiber coordinate system for the 45 deg ply, and fiber failures and matrix splitting between fibers in that ply were predicted based on assumed failure values of 12,200 and 5500 μmm/mm for the strains along and perpendicular to the fiber direction, respectively (see Fig. 4). The stated failure strain values were obtained from quality control static test results in Ref. 11 and do not account for loading rate effects. A faster loading rate will have a minimal effect on the fiber failure strain value (12,200 μmm/mm), and will increase the failure strain level corresponding to matrix splitting between fibers beyond 5500 μmm/mm. The magnitude of the latter increase has not been determined for impact loading rates, and is therefore not accounted for in the attempted failure predictions.

Table 5 presents a comparison of analytically predicted failures with the experimental observations in Ref. 11. With the exception of the third test case, the analytically predicted delamination sizes compare reasonably well with experimental (C-scan) measurements. Also, analytically predicted flexure-induced, back surface failures are in agreement with most of the visual observations made on impacted laminates.[11]

Conclusions

An analysis was developed to study the response of anisotropic laminated plates to low-velocity impact by a rigid object. The analysis assumed a linear variation of the contact force with time, based on experimental test data, until the precipitation of the initial damage ($t=c$). The contact area was also assumed to vary with time, although in an arbitrary manner. Analytically predicted maximum transverse displacements at the impact location ($x=y=0$) at $t=c$ agree well with experimental and finite element results. Computed longitudinal and transverse strains on the back surface ($z=-h/2$) of the impacted laminate, directly below the impact location ($x=y=0$) at $t=c$, also agree well with available experimental results.[11] The validity of the analysis ceases when delaminations are precipitated at $t=c$. The extent of internal damage, predicted using an unsubstantiated failure value for Q_x/h, compares reasonably well with experimental observations. Analytical predictions of concomitant flexure-induced back surface failures at $t=c$ also agree well with experimental observations. Therefore, the developed analysis is believed to be adequate for an initial understanding of the response of laminated plates to low-velocity impact. Its usefulness can be enhanced through the development of empirical relationships for the necessary input parameters and the verification of the employed failure criterion for the prediction of internal damage.

Acknowledgment

The work presented in this paper was accomplished as part of the IR&D activities in the Structural Mechanics Research Department at Northrop Corporation, Aircraft Division.

References

[1]Goldsmith, W., *Impact: The Theory and Physical Behavior of Colliding Solids,* Edward Arnold Publishers, Ltd., London, 1960.

[2]Ramkumar, R. L., "Environmental Effects on Composite Damage Criticality," Naval Air Development Center, Rept. NADC-79067-60, Jan. 1982.

[3]McQuillen, E. J., Llorens, R. E., and Gause, L. W., "Low Velocity Transverse Normal Impact of Graphite-Epoxy Composite Laminates," Naval Air Development Center, Rept. NADC-75119-30, June 1974.

[4]Chou, P. C., Flis, W. J., and Miller, M., "Certification of Composite Aircraft Structures under Impact, Fatigue and Environmental Conditions, Part I: Low Speed Impact of Plates of Composite Materials," Naval Air Development Center, Rept. NADC-78259-60, Jan. 1978.

[5]Whitney, J. M. and Pagano, N. J., "Shear Deformation in Heterogeneous Anisotropic Plates," *Journal of Applied Mechanics,* Vol. 37, 1970, pp. 1031-1036.

[6]Whitney, J. M. and Sun, C. T., "Transient Response of Laminated Composite Plates Subjected to Transverse Dynamic Loading," *Journal of the Acoustical Society of America,* Vol. 61, Jan. 1977, pp. 101-104.

[7]Sun, C. T. and Chattopadhyay, S., "Dynamic Response of Anisotropic Plates Under Initial Stress Due to Impact of a Mass," *Transactions of the ASME, Journal of Applied Mechanics,* Vol. 42, 1975, pp. 693-698.

[8]Dobyns, A. L., "Analysis of Simply-Supported Orthotropic Plates Subject to Static and Dynamic Loads," *AIAA Journal,* Vol. 19, May 1981, pp. 642-650.

[9]Chen, P. C., "Response of Laminated Plates Subjected to Low Velocity Normal Impact," M.S. Thesis, California State University, Long Beach, Dec. 1980.

[10]Jones, R. M., *Mechanics of Composite Materials,* Scripta, Washington, D. C., 1975.

[11]Ramkumar, R. L., "Composite Impact Damage Susceptibility," Naval Air Development Center, Rept. NADC-79068-60, Jan. 1981.

[12]Sneddon, I. N., *Fourier Transforms,* McGraw-Hill Book Co., New York, 1951.

[13]Singleton, R. C., "On Computing the Fast Fourier Transform," *Communications of the Association for Computing Machinery,* Vol. 10, No. 10, 1967, pp. 647-654.

From the AIAA Progress in Astronautics and Aeronautics Series . . .

TRANSONIC AERODYNAMICS—v. 81

Edited by David Nixon, Nielsen Engineering & Research, Inc.

Forty years ago in the early 1940s the advent of high-performance military aircraft that could reach transonic speeds in a dive led to a concentration of research effort, experimental and theoretical, in transonic flow. For a variety of reasons, fundamental progress was slow until the availability of large computers in the late 1960s initiated the present resurgence of interest in the topic. Since that time, prediction methods have developed rapidly and, together with the impetus given by the fuel shortage and the high cost of fuel to the evolution of energy-efficient aircraft, have led to major advances in the understanding of the physical nature of transonic flow. In spite of this growth in knowledge, no book has appeared that treats the advances of the past decade, even in the limited field of steady-state flows. A major feature of the present book is the balance in presentation between theory and numerical analyses on the one hand and the case studies of application to practical aerodynamic design problems in the aviation industry on the other.

696 pp., 6×9, illus., $30.00 Mem., $55.00 List

TO ORDER WRITE: Publications Order Dept., AIAA, 1633 Broadway, New York, N.Y. 10019